Proceedings of the 5th International Symposium on Steel Science (ISSS 2017)
Nov. 13-16, 2017, Kyoto, Japan: The Iron and Steel Institute of Japan

Multi-scaled heterogeneities in elasto-plastic deformation and microstructure in steels

Y. Tomota[1, 2*]

[1] National Institute for Materials Science, 1-2-1, Sengen, Tsukuba, Ibaraki, Japan
[2] National Institute for Advanced Industrial Science and Technology, 1-1-1, Umezono, Tsukuba, Ibaraki, Japan

Abstract: Elasto-plastic deformation occurs heterogeneously in steels, which is caused by anisotropic elastic properties and hierarchically multi-scaled heterogeneous microstructures. In situ neutron diffraction measurements during deformation have revealed the superposition of internal stresses related to multi-scaled eigen (misfit) strains. Intergranular strains and dislocation densities in individual <hkl> oriented grain-families are evaluated for austenite steel, stress partitioning behavior between hard and soft packets in addition to intergranular stresses for martensite steel, and the superposition of intergranular, colony and phase stresses for pearlite steel. In a macroscopic scale, the Lüders deformation are observed in certain advanced steels accompanying martensitic transformation, whose mechanism is open for discussion. Next, the volume fraction of metastable austenite shows the trend to increase when it is determined by TEM, SEM/EBSD, X-ray and neutron, in order, because martensite transformation occurs easily at the surface layer. If the measurement were performed at elevated temperatures, only the result obtained by neutron diffraction agrees with that by dilatometry. The reason why EBSD and X-ray diffraction cannot measure appropriately is the change in C and Mn concentrations near the surface. In situ EBSD monitoring for austenite reversion is useful showing good agreements with the results by in situ neutron diffraction as long as the influence of change in chemical compositions at the surface can be ignored. Changes in peak intensity, shift and broadening of neutron diffraction profile during pearlitic transformation provide new insights for transformation mechanism. Finally, short history on the application of neutron beam experiments to steel science is reviewed.

1. INTRODUCTION

This symposium started in 2007 aiming at (i) a compact one in order to deepen research discussion, (ii) a kind of school with minimum expense, (iii) inviting world-leading scientists for oral presentations, (iv) no parallel session and poster presentations for general contributions, (v) encouraging young researchers to be new leaders and (vi) having pre-seminar for preparation and post-symposium for summary [1]. Then, in this talk, recent topics still open for questions are discussed. It is well known that elasto-plastic deformation occurs heterogeneously in steels caused by anisotropic elastic and plastic properties of constituent phases, i.e. austenite, ferrite and cementite and hierarchically multi-scaled heterogeneous microstructures. Such multi-scaled heterogeneities from atomic level to mechanical test specimen level have well been characterized using advanced techniques like atom probe tomography (APT), transmission electron microscopy (TEM), scanning electron microscopy (SEM) coupled with electron back scattering diffraction (EBSD) or electron channelling contrast image (ECCI), or digital image contrast (DIC) etc. These experimental techniques are quite powerful to identify such heterogeneities but not easy to connect them with macroscopic properties like stress-strain curve. These data are obtained at specimen surface or a tiny sample and hence sometimes suspected to be a little different from the bulk-averaged information. To connect the microstructural data with global phenomena like tensile deformation, bulk averaged values with satisfactory statistics are needed and thereby neutron scattering measurements are quite helpful to bridge these two. Figure 1 explains three kinds of stresses, i.e., Type 1 of macroscopic stress generally used for mechanical design, Type 2 working over <hkl> oriented grains (intergranular stress) or constituent phase (phase stress) and Type 3 corresponding to the internal stress field around lattice defects like dislocation; substructure yields Type 3 stress distribution within a grain of a plastically deformed sample [2, 3]. To be noted here is that the

* Y. Tomota, E-mail: TOMOTA.Yo@nims.go.jp, telephone: +81-298-51-3354 EXT3915

surface layer with a plane stress condition is easier to deform plastically. Hence, after unloading, the macroscopic compressive stress remains near the surface. The continuous monitoring of the surface with deformation by SEM/EBSD, DIC or micro-grid method is useful to obtain the insights on heterogeneous deformation related with microstructure but it is always recommended to compare with relevant bulk-averaged information which can be obtained by neutron scattering or in some cases by synchrotron X-ray scattering, particularly diffraction. A schematic illustration of change in neutron diffraction profile by deformation is drawn in Fig. 2. Changes in diffraction peak intensity associated with crystal rotation or phase transformation, peak shift related to elastic strain/stress, and profile line broadening take place with plastic deformation. In case of heat treatment, the diffraction peak shift occurs also by thermal expansion or contraction and change in concentration of alloy elements like carbon. If the peak shift is related only to elastic strain in Fig. 2, the intergranular strain, ε_{hkl} was calculated from the change in the lattice plane spacing for <hkl> oriented grains-family along the tensile direction, d_{hkl}, by the

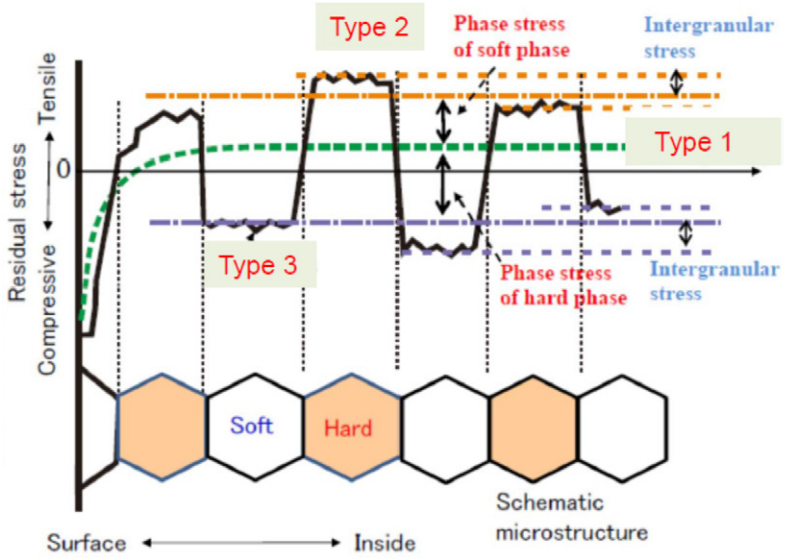

Fig. 1 Schematic illustration to explain the residual stress distribution in the cross section of a plastically deformed two phase steel.

following equation:

$$\varepsilon_{hkl} = \left(d_{hkl} - d^0_{hkl}\right)/d^0_{hkl} \quad (1)$$

where the subscript "0" refers to the stress-free {hkl} spacing. In case of a two-phase steel, the lattice constant of constituent phase, a_{ph} can be determined by multi-peak profile fitting using the Rietveld method, and the phase strain is caluculated by Eq. 2 similarly to Eq. 1.

$$\varepsilon_{ph.} = \left(a_{ph.} - a^0_{ph.}\right)/a^0_{ph.} \quad (2)$$

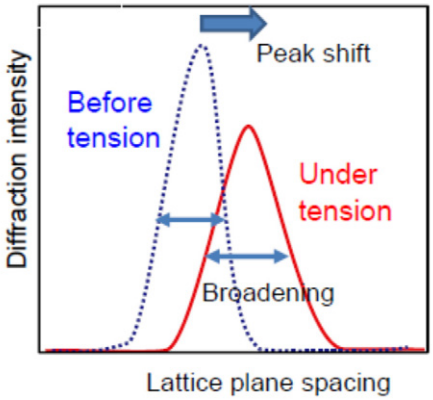

Fig. 2 Schematic illustration of change in diffraction profile with tensile loading.

To be noted is that a_{ph} depends on the direction of scattering vector in a specimen with residual stresses, that is, not true lattice constant of the crystal. Generally, normal strains from different 6 directions are needed to determine stresses σ_{ij} using the following Hooke's law.

$$\sigma_{ij} = C_{ijkl}\varepsilon_{kl} \quad (3)$$

where C_{ijkl} stands for elastic moduli. If the principal stresses directions are known, strains along 3 directions (x_1, x_2 and x_3 axes) would be enough to convert strains to stresses. In case of axial symmetry deformation like tensile test, only the axial and transverse directions can provide phase stresses. The macroscopic stresses (Type 1) can be obtained from phase stresses and volume fractions of constituent phases. For example, in an α-γ steel, the macroscopic stresses, σ_{ij}^{A} can be written as,

$$\sigma_{ij}^{A} = \sigma_{ij}^{\alpha} f^{\alpha} + \sigma_{ij}^{\gamma} f^{\gamma} \quad (4)$$

In case of single phase steel, the phase stress equals to macroscopic stress (Type 1). Sometimes, the difference, $(\sigma_{ij}^{\alpha} - \sigma_{ij}^{A})$ or $(\sigma_{ij}^{\gamma} - \sigma_{ij}^{A})$ is also called phase stress. To be noted here is that the intergranular stress could not be obtained because a certain <hkl> grain-family related to the tensile direction is different from that to the transverse direction.

2. MULTI-SCALED HETEROGENEOUS DEFORMATION BEHAVIOR IN STEELS

2.1. Austenite steel

The view of in situ neutron diffraction measurement during tensile test at J-PARC MLF is presented in Fig. 3. A tensile tester was set in such a way that the tensile direction becomes 45 degrees with respect to the incident beam, so that the diffraction profiles with the scattering vector parallel either to the tensile direction or transverse could be simultaneously recorded by the two detectors shown in Fig. 3. The event data acquisition system has been employed for the time-of-flight (TOF) method at J-PARC MLF and hence a time slicing interval can be changed after the experiment judging from the statistic reliability of the profiles like in Fig. 3(c) and (d). As seen, the diffraction profiles for a deformed SUS 304 steel obtained from the two directions differ from each other exhibiting the texture evolution with tensile plastic deformation: the starting profiles were almost identical in the both directions indicating nearly texture free [4]. As is inserted in Fig. 3 (d), for example, the 200 peak encircled was the sum of diffraction beam intensities from all <200> oriented grains with respect to the transverse direction within the gauge volume of 5 x 5 x 5 mm^3, in which several million grains are involved. Compared with the other diffraction methods using electron beam or X-ray, this neutron diffraction is superior to obtain global averaged information.

The intergranular strains were computed by Eq. 1 inputting the lattice plane spacing obtained before tensile test into d_{hkl}^{0} and the obtained results are presented in Fig. 4 [5]. The deformation is divided into three stages: at the stage 0_p, all grains deform only elastically, at stage I_p some grains deform plastically but the others still only elastically and at stage II_p all grains deform plastically. Such transitions can be found in the applied stress versus <hkl> lattice plane strain curves. As seen, the

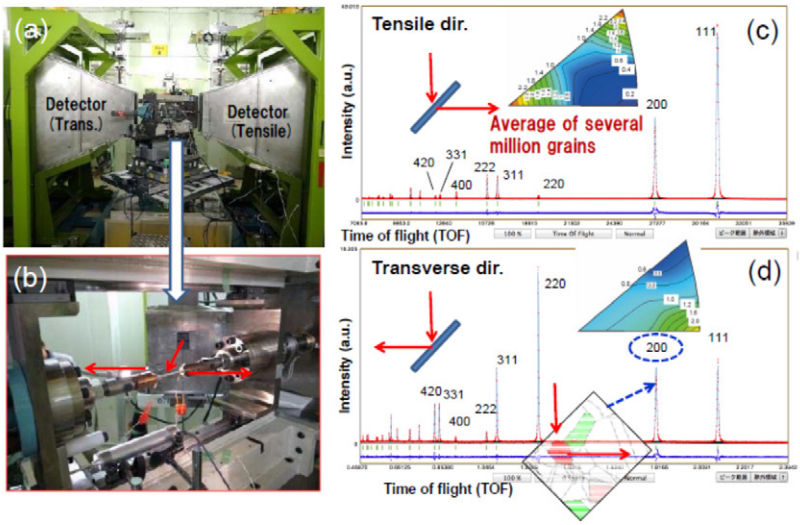

Fig. 3 In situ neutron diffraction measurements during tensile test at BL19 of J-PARC MLF: (a) whole view and (b) the details of a specimen with strain gage and (c, d) examples of obtained diffraction profiles under tensile load with the scattering vector parallel either to the tensile direction or transverse for SUS 304 [5].

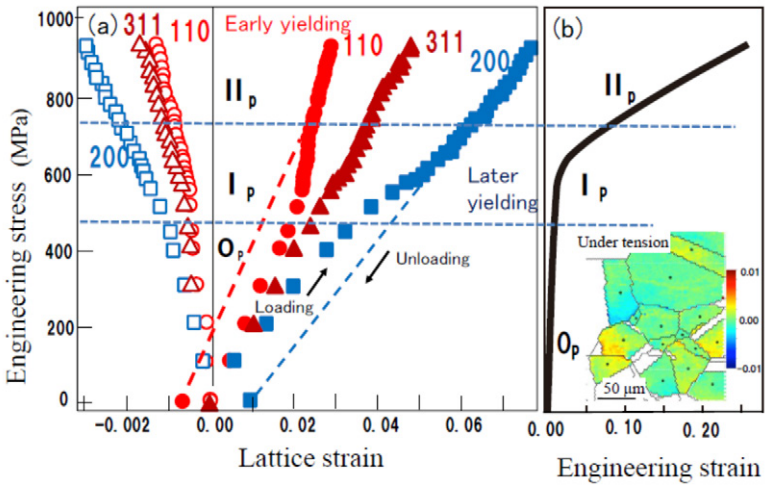

Fig. 4 <hkl> intergranular strains as a function of the applied stress (a) and macroscopic stress- strain curve (b) [5] in which stress distribution determined by EBSD/Wilkinson method [6] is inserted.

increasing rate in the lattice strain for 200 becomes larger whereas that of 110 smaller at stage I_p, which means the occurrence of preferential plastic flow in <110> grain-family. Similar features can be recognized by the surface observations using the Wilkinson method for SEM/EBSD measurement [6] as an example of elastic strain map is inserted in (b). Though the insights obtained by EBSD is easy to identify the inhomogeneous deformation, neutron diffraction is superior to get quantitative data. The changes of intergranular strains along the tensile direction in Fig. 1(a) is not difficult to understand but those along the transverse direction are somewhat puzzling. Here, it is helpful to combine the computer simulation results using an elasto-plastic self-consistent model (EPSC) or crystal plasticity finite element method (CP-FEM) [7]. It is important to put more than 1000 grains into calculation and therefore FFT-CPFEM is very useful. The calculated results show good correspondence with the neutron diffraction results like Fig. 4(a) and behavior in the transverse direction is also well understood.

Dislocation related characteristics can be determined using the convolutional multiple whole profile fitting (CMWP) method [8] for diffraction profiles as a function of tensile strain [9]. The change in dislocation arrangement parameter and character (ratio of edge component to screw) and crystallite size are determined. Here, only the change of dislocation density with tensile deformation is presented in Fig. 5(a). This density is global-averaged value used "mean contrast factor for dislocation" and the density in individual <hkl> grains family is estimated using an individual contrast factor for profile fitting [10]. An example of dislocation density in individual <hkl> grain-family is shown in Fig. 5(b) [9]. It is noted that the density in lower indexed group like 110 is about twice of that in 211. Therefore, both of stress and dislocation density are dependent on the crystal orientation of individual grain. Ungár et al. have claimed the coefficient (α) of Taylor (or Bailey-Hirsch) equation depends on <hkl> by plotting the shear stress (τ) operating for slip system and dislocation density (ρ) [10].

$$\tau = \tau_0 + \alpha\mu b\sqrt{\rho} \qquad (5)$$

where τ_0, μ and b refer to constant, shear modulus and magnitude of Burgers vector,

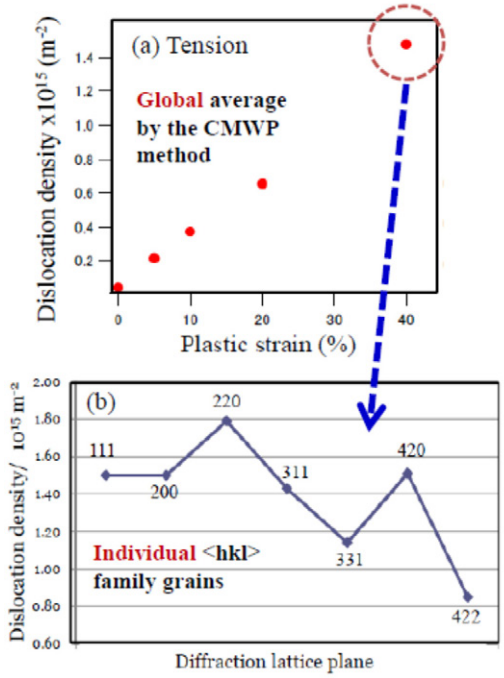

Fig. 5 Schematic illustration to explain the residual stress distribution in a plastically deformed two phase steel [10].

respectively. In case of grain whose orientation locates in the central area of the standard orientation triangle, band structure is evolved to show higher coefficient than that located near 100, 111, etc, in which dislocation cell structure is formed. That is, the α value is influenced of dislocation arrangement. It is, however, not developed to obtain the dislocation arrangement parameter in individual <hkl> grains family by line profile analysis. Another unsolved issue includes that dislocation density determined by line profile analyses is influenced by the measuring direction, i.e., scattering vector. Because the magnitude of intergranular stress is larger and uniform in all <hkl> oriented grains in the tensile direction but not uniform in the transverse direction. This is because only line broadening is used to evaluate dislocation density, neglecting the intergranular stresses. Dislocation substructure brings diffraction peak shift as well as broadening. Quantitative evaluation method for such issues should be more investigated. In conclusion, a polycrystalline single phase material is regarded to be an extreme type of composite material.

2.2 Martensite steel

The typical microstructure of lath martensite is illustrated in Fig. 6 which hierarchically consists of lath, colony, packet and prior austenite grain. In addition to intergranular stress like in austenite steel described above, the packet stress is overlapped when plastically deformed. The results of tensile test for micro-specimens as drawn in Fig. 6, have revealed that the flow stress of a specimen prepared parallel or perpendicular direction to the lath boundary is much higher than those with 45 degrees [11]. That is, there is soft packet (SC) and hard one (HC) related to lath boundary inclination related to tensile direction. Such a packet unit of heterogeneity in plastic deformation was found to bring anisotropy in diffraction profile. Then, packet strains were determined using double peak fitting [12] for diffraction profile and the corresponding strains were determined by

$$\varepsilon_{SC} = \left(d^{S}_{hkl} - d^{0}_{hkl}\right)/d^{0}_{hkl} \quad (6)$$

$$\varepsilon_{HC} = \left(d^{H}_{hkl} - d^{0}_{hkl}\right)/d^{0}_{hkl} \quad (7)$$

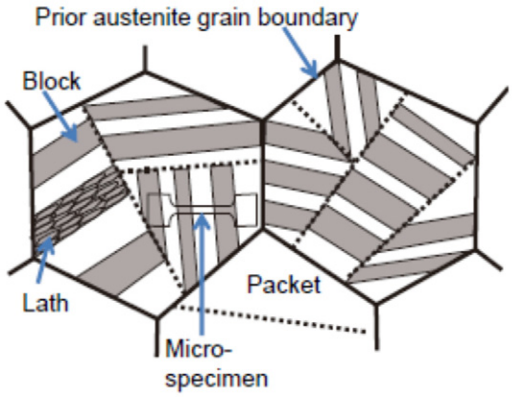

Fig. 6 Schematic illustration of lath martensite which is composed of lath, colony, packet and prior austenite grain [11].

where d^{S}_{hkl}, d^{H}_{hkl} and d^{0}_{hkl} mean hkl plane spacing for SC, that for HC and stress-free, i.e., before deformation, respectively. It is interesting that the full width at a half maximum (FWHM) of diffraction profiles decreases with plastic deformation. However it does not mean that dislocation density decreases but dislocation arrangment changes with plastic deformation. In moe details obtained by CMWP method, as shown in Fig. 7(a), the dislocation density is found to decrease in the soft packet whereas increase in

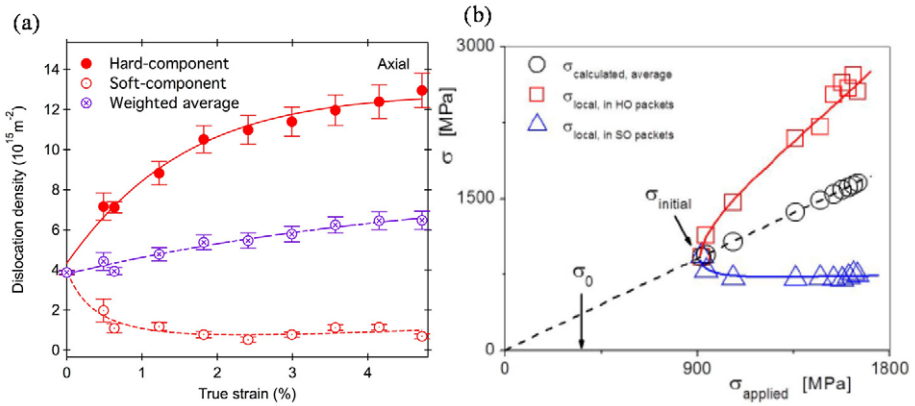

Fig. 7 Dislocation densities in the hard and soft packets as a function of tensile strain (a) and stress partitioning behavior between the two packets (b) [13].

the hard packet. Figure 7(b) depicts the stress partitioning behavior between the two packets [13].

2.3 Pearlite steel

In case of pearlite structure consisting of ferrite and cementite lamellae, its heterogeneous deformation is characterizing by the superposition of multi-scaled stress partitioning, i.e., between ferrite and cementite phases (phase stress), <hkl> oriented grain-families with respect to the tensile direction (intergranular stress) and colonies with different lamellar alignments (colony stress) [14]. The colony stress was evaluated from the asymmetry of profiles similarly to the case of lath martensite described above. Figure 8 presents such superposition of intergranular, phase and colony strains. The change in FWHM was also found different between the two colonies; it hardly increased in the soft colony with tensile deformation whereas increased rapidly in the soft colony, suggesting the increase of dislocation density.

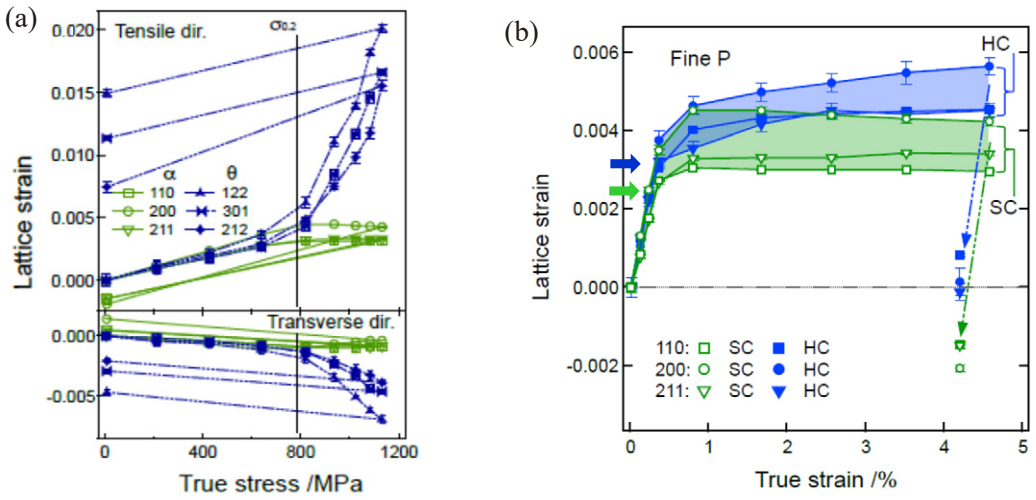

Fig. 8 Multi-scaled stress partition behavior in a pearlite steel: (a) intergranular strains in ferrite and cementite phases in the tensile and transverse directions, where the average of intergranular strains are phase strains and (b) colony strains in which the intergranular strains are also overlapped [14].

2.4 Multi-microstructure steel and Lüders deformation

In case of two ductile phase steel like austenite-ferrite duplex stainless steel and DP steel, the deformation stages A, B and C could be determined from lattice strain versus tensile stress curves. Both constituent phases deform elastically at stage A, only softer phase deforms plastically at stage B and both phases deform plastically at stage C. The stage 0_p, 1_p and 2_p for single phase steel are overlapped for each constituent phase. In TRIP steels, deformation induced martensite transformation is overlapped onto such complicated deformation stages. Phase stress partitioning behavior between ferrite-bainite, austenite and martensite during tensile deformation was determined by in situ neutron diffraction with precise line profile analysis [15].

To achieve high strength without losing ductility, many investigations to develop ultra-fine multi-phase microstructure steels have been performed. It is noted in many cases that the uniform elongation disappears with decreasing of grain size to sub-micron meters because of poor dislocation accumulation ability i.e., low work-hardening. To overcome this drawback, several attempts have been made to increase work-hardening including multi-phase design (phase stress), TRIP, TWIP, etc. Interestingly, in such steels with ultra-high yield strength, discontinuous yielding often takes place accompanying the Lüders band deformation. Stress-strain curves may be classified like in Fig. 9(a) [16]. The magnitude of Lüders strain is empirically summarized in Fig. 9(b) which indicate the work-hardening is balanced with the decrease in specimen cross area in the Lüders band (compare regions A and B in the inserted micrograph) [17]. The transition from continuous (Type IV) to discontinuous yielding (Type III) behavior in high strength-ductile steels are open for discussion. Even in cases of fine structured steels, Type IV deformation has been observed, for example, in nano-bainite, Q&P and pearlite steels. The microstructural criterion for the onset of discontinuous deformation is not made clear.

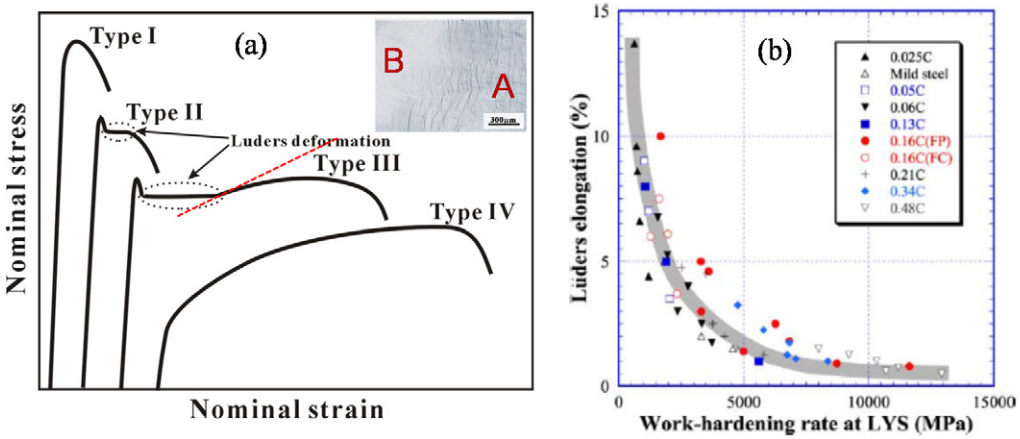

Fig. 9 Classification of stress-strain curves (a) and relationship between Lüders strain and work hardening rate (b) [16, 17]. The inserted micrograph shows the Lüders band observed in a nano-TRIP steel, where region labelled A was work-hardened (inside the band) while B not plastically deformed.

3. CHRACTERIZATION OF MICROSTRUCTURES

3.1 Quantitative evaluation of the volume fraction of the retained austenite

In recent investigations on high strength steels, the retained austenite has been utilized and hence its characterization is a crucial issue. Because metastable austenite transforms easily near the surface or during preparing a tiny sample for TEM observation or APT measurement, the volume fraction determined has sometimes a trend to increase by TEM, EBSD, X-ray and neutron in order [18, 19]. Table 1 is an example of comparison of austenite volume fractions determined by various methods [20]. In this steel, the volume fraction determined by neutron diffraction is comparable with that by X-ray diffraction but much larger than those by EBSD and TEM. To be noted here is that the obtained volume fraction is influenced by the measuring direction commonly for neutron, laboratory X-ray and synchrotron X-ray diffraction. The conventional modification using theoretical diffraction intensities is not enough to remove the influence of texture. As results, it is recommended to measure texture and austenite volume fraction, simultaneously.

Table 1 Austenite volume fraction (%) determined by various methods

	TR1	TR2
Neutron		
Texture	14.8	13.9
Averages	14.6	13.8
Gandolfy	16.3	15.3
ND	11.3	13.8
RD	13.0	14.2
TD	15.0	14.1
Synchrotron		
ND	10.9	9.0
RD	13.6	12.6
TD	15.2	15.9
Labo X-ray		
ND	12.2	12.7
RD	13.7	13.4
TD	14.3	15.4
EBSD	6.4	5.5

For “Texture” and “Average”, diffraction profiles from 526 directions were used.

2.2 Monitoring of transformation by in situ neutron diffraction

Neutron diffraction is believed to be the most suitable method to determine the bulky averaged values of microstructural parameters. Such a feature becomes more attractive to monitor the microstructure evolution during material processing. Many investigations concerning phase transformations, precipitation, recrystallization etc. have been reported using neutron diffraction, so far [5], among which reverse austenite transformation in ferrite-bainite-austenite (or cementite) steel and tempered lath martensite steel, and pearlitic transformation behavior are explained below as recent topics.

(1) Austenite reversion of Fe-Mn-Si-C steels monitored by four different methods

Microstructural changes with annealing for ferrite-bainite-austenite (or cementite) Fe-Mn-Si-C steels were monitored in situ using SEM/EBSD observation, X-ray diffraction and neutron diffraction as well as conventional dilatometry [21]. The obtained results are summarized in Fig. 10 revealing that the result by neutron diffraction agrees well with that by dilatometry but that those by EBSD and X-ray

are much different. The reason why the latter two methods showed higher austenite reverse temperature is the change in chemical compositions near the surface. The depth profile of chemical compositions of the specimen after the EBSD measurement was examined by rf glow discharge optical emission spectroscopy. Mn and C concentrations are lowered in the region from the surface to approximately 3 μm in depth. The chemical compositions examined at the surface by EDS analysis have also revealed that C and Mn contents were lowered after heating for in situ EBSD measurement. Therefore, in addition to decarburizing, Mn atoms were easily desorbed from the surface in a high vacuum due to its higher equilibrium vapour pressure. Similar change in chemical compositions was found together with oxidation near the surface for high temperature X-ray diffraction in a helium gas atmosphere. Hence,

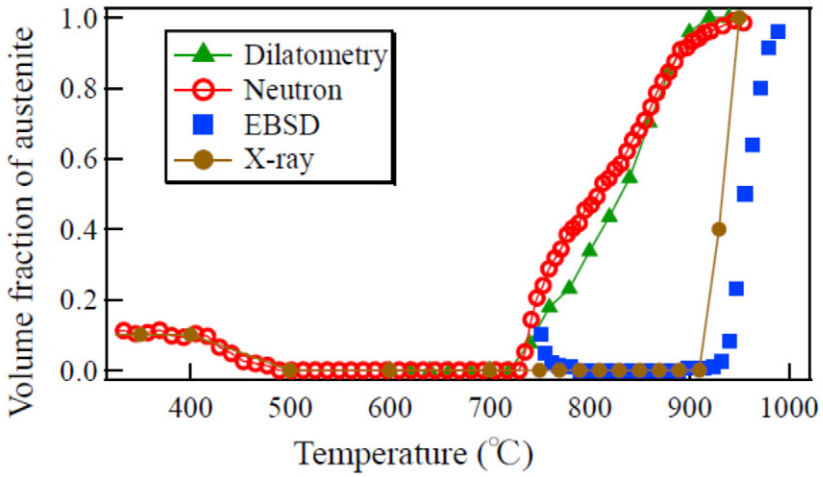

Fig. 10 Change in austenite volume fraction with annealing measured by dilatometry, neutron diffraction, SEM/EBSD and X-ray diffraction [21].

the results by EBSD or X-ray should be understood as the result of Fe-Si alloy not Fe-Mn-Si-C.

(2) Austenite memory phenomenon observed by in situ EBSD and neutron diffraction

As mentioned above, neutron diffraction is a powerful tool to monitor microstructure change at elevated temperatures but always needs complementary information by microstructure observations for interpretation of line profile analysis. If the influence of desorption of Mn and/or C was negligible, the in situ observation with SEM/EBSD would be very helpful to deepen the understanding of neutron diffraction results [22, 23]. As such an example, so-called austenite memory was studied by these two in situ monitorings. The austenite reversion behavior in a tempered martensite steel containing mainly Cr carbide was monitored. In situ EBSD observation revealed two types of austenite nucleation; one is from lath boundary, type A, and the other is from prior austenite grain boundaries or cementite particles, type B. When the type A nucleation is dominant, the reversed austenite grain becomes as large as prior austenite grain showing austenite memory. Austenite grains nucleated within a certain prior austenite grain have almost the same variant. Then, with further annealing after austenite reversion, small number of Type B grains grow preferentially invading the Type A austenite region to be a relatively small sized polygonal structure, similar to recrystallization. In situ neutron diffraction revealed that a high dislocation density in the reversed austenite first and then a low density after further annealing where all <hkl> diffraction intensities became lower due to the primary extinction. In this case, the results by EBSD, neutron and dilatometry are in good agreements.

(3) Pearlitic transformation

As an example of monitoring of phase transformations, the case of pearlitic transformation [24] is explained here. In situ nuetron diffraction measurments were carried out for a high carbon steel during heat treatment: heating up to 1173 K for austenitization followed by isothermal holding below A_1 temperature. As shown in Fig. 11, the austenite lattice constant is found to decrease with not only lowering holding temperature but also during isothermal holding. Because pearlitic transformation accompanies expansion, internal stresses in the untransformed austenite region should be tensile

hydrostatic stress but the result in Fig. 11(a) is opposite. This indicates that the carbon concentration in untransformed austenite region would decrease with the progress of pearlitic transformation. This is postulated to be related to some TEM observations: the thickness of cementite plate becomes thinner, sometime terminates during its growth, i.e., cementite volume fraction decreases with the progress of transformation. Another interesing result is that FWHM of ferrite phase becomes larger with decreasing of transformation temperature. The amount of increase in FWHM caused by thermal misfit strain upon cooling to RT was approximately 20% of those found in Fig. 11(b) and hence large FWHM of ferrite diffraction peak observed at RT is believed to stem from the misfit strains at semi-coherent ferrite/cementite interface. More details will be reported in near future [24].

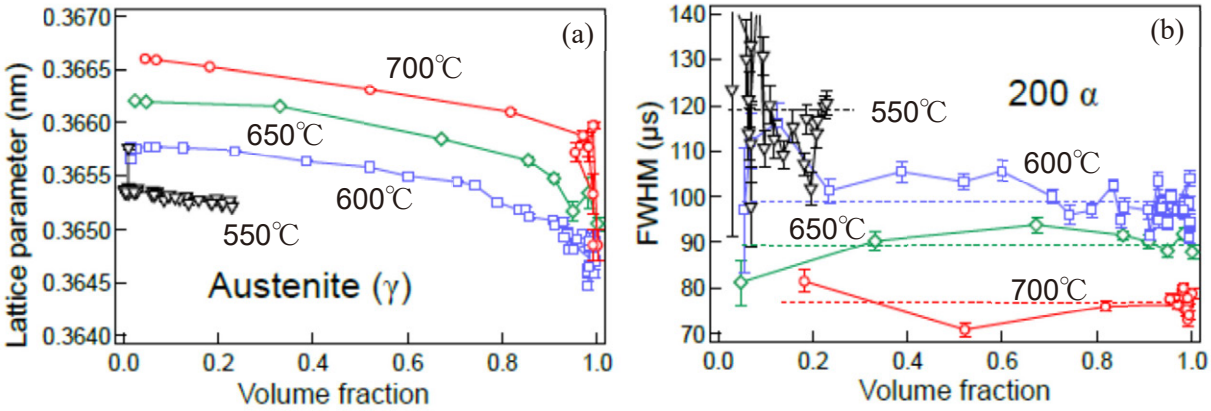

Fig. 11 Changes in austenite lattice constant (a) and FWHM of ferrite 200 reflection (b) during pearlitic transformation at isothermal holding at various temperatures for a high carbon steel [24].

4. CONCLUDING REMARKS

Microstructural characteristics have been elucidated by TEM, SEM/EBSD and/or 3D-APT, but it is also important to measure the bulk-averaged data using neutron and/or synchrotron X-ray diffraction. Small angle neutron scattering, transmission neutron Bragg edge imaging and neutron reflectivity measurement have also been demonstrated to be powerful tools [5]. As is summarized in Fig. 12 [25], the application of neutron beam to steel research has started quite recently compared with electron or X-ray beam, but has rapidly expanded to industrial topics [26]. As results, the competition to get beam time at J-PARC MLF becomes quite severe. Therefore, in order to use neutron beam more freely, much attention has been paid to compact neutron source as complementary use with a large facility like J-PARC. In actual, the compact neutron sources of HUNS and RANS in Fig. 12 have demonstrated to provide valuable measurements and a new compact neutron source aiming at industrial use is under

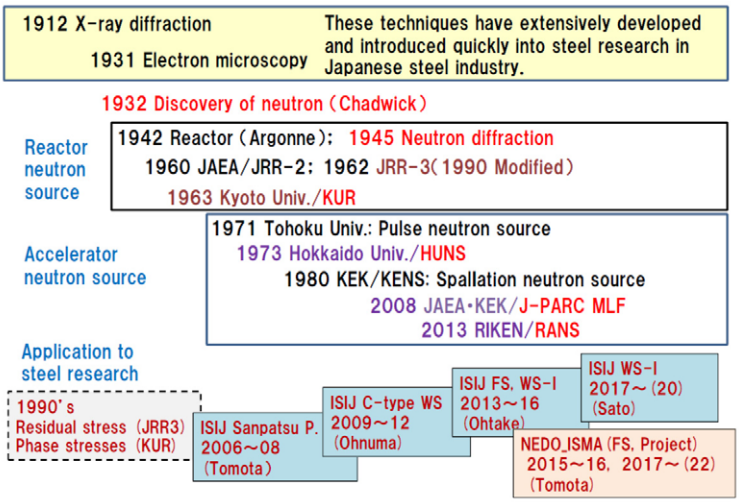

Fig. 12 History of neutron beam experiments for steel research in Japan [25]

construction in the ISMA project (Fig. 12). Therefore, in near future, the use of neutron experiments is expected to be a kind of daily work because of easy sample preparation.

Acknowledgements: The author wish to thank the following co-workers for their helpful and patient works: Drs. S. Harjo, S. Morooka, P.G. Xu, T. Kawasaki, Y.H. Su, K. Aizawa: Japan Atomic Energy Agency, W. Gong: Kyoto University, Y. Adachi, Nagoya University, M. Ojima: JFE steel Co., T. Shinozaki: Kobe steel Co., A. Taniyama: Nippon Steel and Sumitomo metal Co., T. Fukino: TSL solutions Ltd., N. Sekido, T. Ohmura: National Institute for Materials Science, T. Suzuki, S. Sato: Ibaraki University, Y.X. Wang: Kyusyu University, P. Lukas: Nuclear Physics Institute and T. Ungár: Eötvös University and others.

REFERENCES

[1]Y. Tomota and K. Tsuzaki: Ferrum (ISIJ), 14(2009), 79-80.
[2] M.E. Fizpatrick and A. Lodini: Analysis of Residual Stress by Diffraction using Neutron and Synchrotron Radiation, Taylor & Francis, (2003).
[3] M.T. Huchings, P.J. Withers, T.M. Holden, T. Lorentzen: Introduction to the Characterization of Residual Stress by Neutron Diffraction, CRC Press, Taylor & Francis, (2005).
[4] Y. Tomota, S. Harjo: J. Jpn Soc. Plasticity, 54(2013), 891-895.
[5] Y. Tomota: Materia Japan, 56(2017), 14-19; 56(2017), 70-75; 56(2017), 296-301.
[6] M. Ojima, Y. Adachi, S. Suzuki, Y. Tomota: Acta Mater., 59(2011), 4177-4185.
[7] A.K. Kanjarla, R.A. Lebensohn, L. Balogh, C.N. Tome: Acta Mater., 60(2012), 3094-3106.
[8] T. Ungár, J. Gubicza, G. Ribárik, A. Borbely: J. Appl.Cryst., 32(1999), 992-1002; G. Ribárik and T. Ungár; Mater.Sci.Eng., A528(2010), 112-121, eCMWP: http://www.renyi.hu/cmwp (available on Nov. 9, 2017)
[9] Y. Tomota, S. Sato, S. Harjo, W. Gong: to be submitted (presented at MECA SENS 8 (2015)).
[10] T. Ungár, A.D.Stoica, G.Tichy, X-L.Wang: Acta Mater., 66(2014), 251-261.
[11] K. Kwak,T. Mayama, Y. Mine, K. Takashima: Mater. Sci. Eng. A, 674(2015), 104-116.
[12] T. Ungár, S. Harjo, T. Kawasaki, Y. Tomota, G. Ribárik, Z. Shi: Metall.Mater.Trans.A, 48(2017), 159-167.
[13] S. Harjo, T. Kawasaki, Y. Tomota, W. Gong, T. Ungar, K. Aizawa, Z. Shi: Mater. Metall. Trans. A, 48(2017), 4081-4092.
[14] Y.X. Wang, T. Ohnuki, Y. Tomota, S. Harjo, M. Ohmura: Scripta Mater., 140 (2017) 45-49.
[15] S. Harjo, N. Tsuchida, J. Abe, W. Gong: to appear in Scientific Report, (2017):| DOI:10.1038/s41598-017-15252-5
[16] K. Asoo, Y. Tomota, S. Harjo, Y. Okitsu: ISIJ Int., 51(2011), 145-150.
[17] N. Tsuchida, Y.Tomota, K,Nagai, K. Fukaura: Scripta Mater., 54(2006), 57-60.
[18] S. He, Y. Tomota, Y.H. Su, W. Gong, S. Harjo, Z. Zhao: ISIJ Int., 55(2015), 686-690.
[19] P.G. Xu, Y. Tomota, Y. Arakaki, S. Harjo, H. Sueyoshi: Mater. Characterization, 127(2017), 104-110.
[20] Y. Tomota, N. Sekido, P.G. Xu, T. Kawasaki, S. Harjo, M. Tanaka, T. Shinohara, Y.H. Su, A. Taniyama: Tetsu-to-Hagané, 103, (2017), 573-581.
[21] Y. Tomota, N. Sekido, S. Harjo, T. Kawasaki, W. Gong, A. Taniyama: ISIJ Int., 57 (2017), 2240-2247.
[22] Y. Tomota, W. Gong, S. Harjo, T. Shinozaki: Scripta Mater., 133(2017), 79-82.
[23] T. Shinozaki, Y, Tomota, T. Fukino, T. Suzuki: ISIJ Int., 57(2017), 533-539.
[24] X.Y. Wang, Y. Tomota, W. Gong, S. Harjo, A. Paradowska, T. Ohmura: to be submitted.
[25] Y. Tomota: Ferrum (ISIJ), 21(2016), 380-384.
[26] K. Sato, H. Nakamichi and H. Sueyoshi: Physics World, (2017), October, http://live.iop-pp01.agh.sleek.net/physicsworld/reader/#!edition/editions_neutron_2017/article/page-22576 (available on Nov. 9, 2017, 11 pages).